Imaging of Surface Plasmon Scattering by Lithographically Created Individual Surface Defects

Igor I. Smolyaninov, David L. Mazzoni, and Christopher C. Davis
Electrical Engineering Department, University of Maryland, College Park, Maryland 20742
(Received 12 February 1996)

A new technique for direct-write ablation on a 100 nm scale has been implemented in a photon scanning tunneling microscope setup. This combination allows us, for the first time, to study surface plasmon scattering by *in situ* created individual surface defects, while the sizes and shapes of the defects are varied. It is found that, within a certain range of size, a hill on an otherwise flat surface can be a source of a micrometer wide plasmon beam. Another new observation is that the effective cross section of a defect can be substantially larger than its visible geometrical size. These results suggest possible practical applications of surface plasmons in two-dimensional optical arrangements. [S0031-9007(96)01521-9]

PACS numbers: 73.20.Mf, 61.16.Ch

The surface plasmon (SP) is a fundamental electromagnetic excitation mode of a metal-dielectric interface [1]. The electromagnetic field of the SP decays exponentially with distance from the interface into each of the bounding media. The SP is free to propagate along the metal surface. Its mean free path is determined by the quality of the surface and Ohmic losses. If the surface is perfectly flat then Ohmic loss is the only channel for decay since the momentum conservation law prohibits SP conversion into photons. In the visible range the SP mean free path on a silver surface is limited to about 50 μm but can extend to many mm in the infrared region. Similar waves exist on the surfaces of a number of dielectrics and semiconductors. Since the properties of SPs depend strongly on the properties of the interface along which they propagate, they have found applications in surface analysis [1]. But until recently there was no tool for the direct study of SP propagation, since the SP field decay length perpendicular to the interface is on the order of 100 nm in the visible range. The development of near-field scanning optical microscopy (NSOM) has opened the way to probe the SP field [2,3] above the surface and to visualize its distribution [4,5]. The extension of SP studies to the control of SPs by two-dimensional optics is anticipated. However, to date, there has been no attempt to create a real two-dimensional optical element for SPs.

We have developed a novel direct-write lithography technique that allows us to create submicron size patterns on virtually any opaque surface. This technique implements a standard NSOM/shear force microscope (our version of this microscope is described in [6]). The use of uncoated UV grade tapered fiber and nanosecond pulsed 248 nm excimer laser light allows us to deliver an estimated 200 GW/m^2 UV light power into a tip-sample region smaller than 200 $\times$ 200 nm^2 during a single laser pulse. This power is sufficient for local surface ablation of gold or silver and local melting of silicon without melting of the transparent UV fiber tip [7]. The topographic changes caused by UV irradiation are immediately recorded by the shear force microscope. The developed technique is to some extent similar to scanning tunneling microscopy lithography but is not restricted by the conductance of the sample surface. We have implemented our lithography technique to study the scattering of surface plasmons by *in situ* created individual surface defects and to create some prototype two-dimensional optical elements for SPs.

In our experiment, SPs are excited in an attenuated total reflection (ATR) arrangement [8] on the surface of an 80 nm thick silver film evaporated onto the hypotenuse face of a right angle glass prism (Fig. 1). An unfocused He-Ne laser beam is used for the excitation of the SPs. Wave vector matching to the SP mode at the silver-air interface is achieved when light is internally incident on the silver film at an angle $\alpha = \arcsin\{[\epsilon_{Ag}/(\epsilon_g\epsilon_{Ag} + \epsilon_g)]^{1/2}\} = 42°$, where ϵ_{Ag} and ϵ_g are the dielectric constants of silver and the glass prism (this value stems

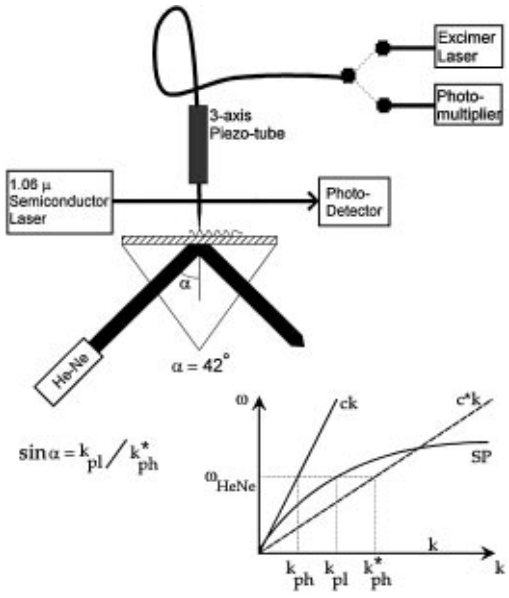

FIG. 1. Schematic view of the experimental setup. Dispersion curves for surface plasmons and photons in air and in glass are shown in the inset.

from the SP dispersion relation in the thick film limit [4]). The thickness of the film is slightly less than the decay length of the SP field into silver, so the coupling of fields between the top and bottom interfaces is sufficient for effective SP excitation. The SP local field is probed with an uncoated adiabatically tapered fiber tip which is drawn at the end of 200 μm UV fiber by heating it with a CO_2 laser beam in a micropipette puller. The fiber tip can be scanned over the sample surface with a constant tip-surface distance ($\sim$5 nm) by the shear force feedback described elsewhere [6]. Therefore, surface topography can be imaged with a resolution on the nanometer scale, while simultaneously recording a near-field optical image corresponding to a distribution of the SP local field intensity near the film surface. This configuration of a near field microscope is usually called a photon scanning tunneling microscope (PSTM) [9]. For the purpose of lithography the free end of the fiber can be connected to the output of the 248 nm excimer laser. The laser power is easy to attenuate in order to change the size of defects in the film.

We present images of the optical near field around *in situ* created single defects having different shapes and sizes. These images result from the scattering of the SP field by the defects. They also contain an evanescent component of the totally internally reflected He-Ne laser beam used for the excitation of SPs. But this evanescent component does not propagate along the surface, so one can distinguish its contribution from the contribution of SP field scattering. The internal halftone contrast is used in the images with the difference from black to white corresponding to the difference between the lowest and the highest level of the optical signal in the image.

At maximum laser power, a single nanosecond UV pulse delivered to the silver film surface by the uncoated tapered fiber was able to ablate a hole through the 80 nm thick film. The topography of such a defect looks like a crater with an approximately 0.5 μm hole in the middle. The optical near field has a strong maximum around the hole because the glass prism surface is almost clear of metal in the hole, and we see the near field of the totally internally reflected He-Ne laser beam used for the excitation of SPs. By attenuating the UV laser pulse power we are able to make craters of shallower depth and smaller diameter. Craters may even disappear and lead to a hill at the irradiated site. Such hills created at approximately $\frac{3}{4}$ of the initial power are shown in Fig. 2. Strong maxima of the optical near field are again seen around these hills. The surprising new feature of the near-field image in Fig. 2(b) is the appearance of quite strong and narrow beams (their cross section is about 1 μm) shining from the hills in the direction determined by the He-Ne laser beam used for SP excitation. These "beams" are localized within the surface. The near-field intensity seems not to change significantly along the 7 μm length of the left "beam" visible in the image. On the other hand, a far-field image taken 7 μm away from the surface appears completely dark on the same halftone scale. A number of images taken at intermediate distances show exponential attenuation of the beam "brightness" with the increasing distance from the surface. Evidently, we see surface plasmon beams shining from the peaks of the optical near field around the hills. We refer to these structures as plasmon "flashlights."

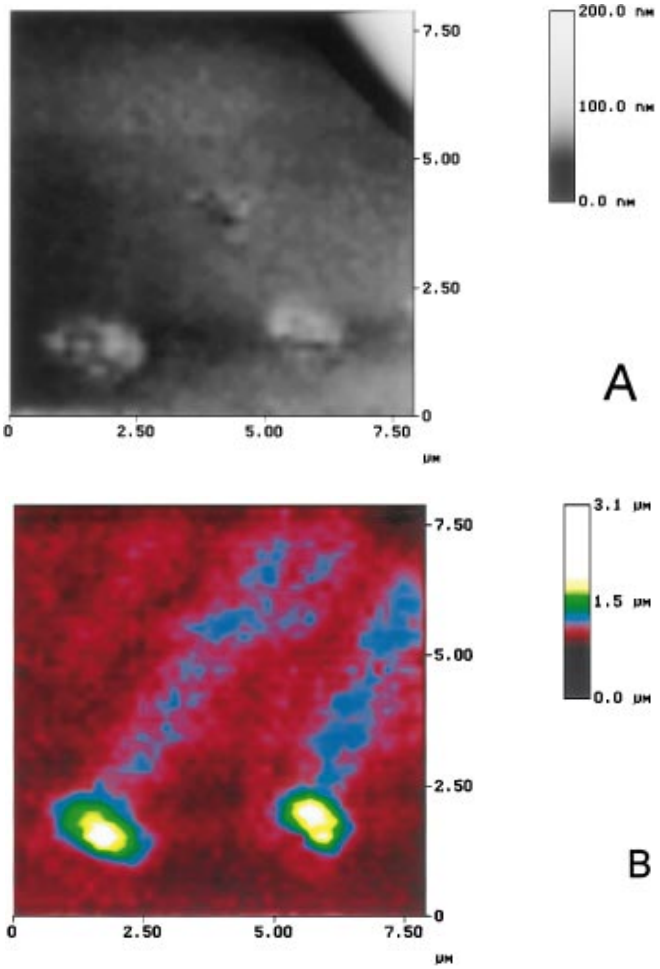

FIG. 2. Topography (a) and optical near-field distribution (b) (color) around two plasmon flashlight structures. The upper right corner of image (a) is an artifact caused by feedback saturation.

In order to understand why a plasmon "flashlight" structure is possible, we should remember that at a given frequency the momentum of a surface plasmon is larger than the momentum of photons in a vacuum. In our ATR geometry, plasmons gain their momentum from photons in a glass prism that have larger momentum. So, the direction of plasmon propagation is determined by the direction of the incoming He-Ne laser beam. Defects of the surface can destroy plasmons, since the momentum conservation law is no longer valid in the vicinity of a defect (a defect breaks translational symmetry of the surface). But, because of the reciprocity theorem, defects

can also increase the plasmon creation rate by photons. Although the coupling conditions are worse around the hills in Fig. 2 (phase matching conditions are corrugated), the strength of the near-field maxima around the hills provides stronger overall coupling between photons in glass and surface plasmons. This fact is actually used in another experimental technique for plasmon excitation: edge diffraction geometry [10]. In this geometry, plasmons are excited by a laser beam shining at some defect (for instance, a razor blade edge) that is brought close to the metal surface. The plasmons are created near the defect and propagate along the direction of the laser beam. Wide plasmon beams generated in such a geometry were used in SP Fourier spectroscopy [1]. Still, it is quite surprising that it is possible to create such a well defined micrometer wide plasmon beam on the surface. One can anticipate the use of such flashlights in miniaturized surface chemistry sensors.

Further attenuation of the UV power during the lithography process allows us to create smaller surface defects and study plasmon scattering by these defects. The results of these studies are shown in Fig. 3. The UV power used to create these smaller defects was approximately $\frac{1}{2}$ of the initial power. We cannot see bright near-field maxima around these defects anymore. Instead, we see prominent shadows behind the defects (the direction of plasmon propagation is shown by the arrows). Two characteristic features of these figures emerge. The sources of the shadows appear to be larger in the near-field images than might be expected from the topography. [Comparison of these images with the near-field image in Fig. 2(b) shows that this effect does not stem from the resolution of the near-field images.] Also, the shadows have an angular shape with different but rather large angle values. The angle values cannot be accounted for by diffraction. The diffraction angle can be easily estimated from the uncertainty principle: $\beta \sim \delta k_{\mathrm{pl}}/k_{\mathrm{pl}} \sim \lambda_{\mathrm{pl}}/(2\pi d)$, where $\lambda_{\mathrm{pl}} = 590$ nm is a plasmon wavelength and d is the size of a scatterer. A micrometer size scatterer gives diffraction angle values on the order of 5°. This value is consistent with the rather small visible width of the SP beams in the plasmon flashlights in Fig. 2.

The simplest explanation of the observed discrepancy between the visible sizes of the shadow sources in the near-field and topographic maps could be that the actual size of the scatterers is not the one that is seen in the surface topographic map. The bulk structure of the silver film can be deformed around the surface defect. Also, the chemical composition of the surface oxide layer (and/or absorbed layer) could be changed under UV irradiation on a much larger scale than the visible size of the defect. Precise control of these parameters would require experiments under ultrahigh vacuum conditions. But, there is also strong theoretical evidence that the

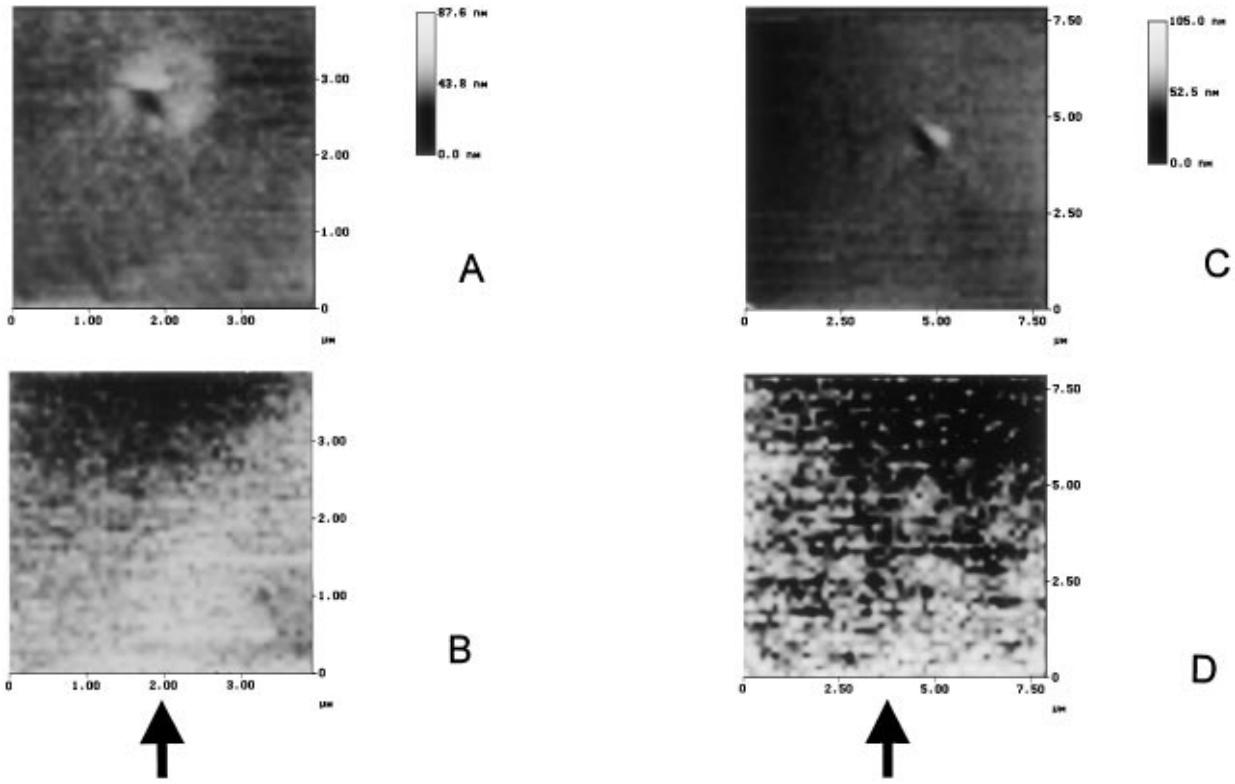

FIG. 3. Topography (a),(c) and optical near-field distribution (b),(d) around smaller defects created at about $\frac{1}{2}$ of the initial power. The direction of plasmon propagation is shown by the arrow. Shadows are seen behind the defects.

visible size of even a point scatterer in the near-field map may be on the order of some micrometers. Let us imagine a point defect on an otherwise ideally flat metal film surface. This defect is irradiated by a plane surface plasmon wave. The defect breaks translational symmetry of the film surface. The SP wave can transfer part of its momentum to the defect and decay into a photon. Consider the cross section of the point defect for such a process. This point defect can be Fourier decomposed into a set of diffraction gratings with periods from zero to infinity (in reality, the upper limit is the inverse atomic size). Since SP scattering is a linear process, we can treat the SP interaction with each diffraction grating separately. Each grating can change the momentum of a plasmon by a multiple of its inverse period. Most probably the plasmon momentum will change by only one inverse grating period. If the inverse grating period is smaller than the difference between the momentum of plasmon and the momentum of photon, then plasmon decay will not happen. Hence, only gratings with sufficiently large inverse periods will interact with the plasmon. In order to find the cross section of the point defect, we should cut off the Fourier spectrum of the defect at wave vectors less than the difference between the plasmon and photon wave vectors $(k_{\mathrm{pl}} - k_{\mathrm{ph}})$ and perform an inverse Fourier transformation. Such a procedure gives an effective cross section $s \sim 1/(k_{\mathrm{pl}} - k_{\mathrm{ph}})$. This cross section is $s \sim 1.6\ \mu$m at He-Ne laser wavelengths. This value is consistent with the effective sizes of the shadow sources in Figs. 3(b) and 3(d).

The cross section s is, in fact, only the cross section for an inelastic process: the decay of a plasmon into a photon. The elastic cross section s_e of plasmon to plasmon conversion could be larger. In this process the plasmon changes its propagation direction, but the value of its momentum remains the same. Similar to inelastic scattering, the elastic cross section for the deflection of a plasmon at an angle β in the Born approximation is determined by the Fourier component of the scatterer at the momentum transferred $\delta k = 2k_{\mathrm{pl}} \sin(\beta/2)$. The symmetry between deflection at angles β and $-\beta$ is broken when the real SP wave packet (instead of the plane wave) passes by the defect with a nonzero collision parameter. These reasons could explain qualitatively the angular shape of the shadows in Fig. 3, although these angles are still rather large. The scattering of a surface plasmon from a point defect remains an unsolved theoretical problem.

We have used created surface defects to make another simple two-dimensional optical element that we refer to as a "beam stop." The SP field distribution around this element is shown in Fig. 4. A number of defects similar to the one in Fig. 3(c) were created along a single line at distance about 1 μm from each other. The near-field image shows some increase in the optical field around the defects and a prominent dark shadow behind the line of defects. Thus, an effective optical shield has been created that does not allow plasmons to pass by.

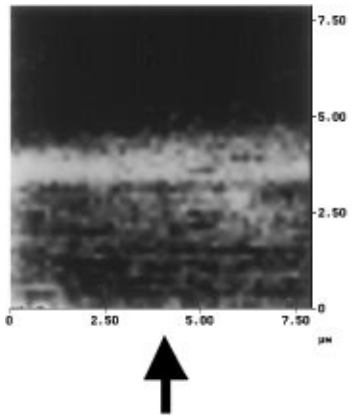

FIG. 4. Optical near-field distribution around a plasmon beam stop structure.

In summary, we have constructed a novel combined PSTM/direct-write lithography setup that has allowed us to study the scattering of surface plasmons by individual defects, while continuously adjusting their shapes and sizes. We have demonstrated simple prototype SP optical elements such as the plasmon flashlight and beam stop. We believe our technique has the potential to create analogs of any three-dimensional optical devices in two dimensions. Similar techniques can be used not only in the two-dimensional optics of surface plasmons on metal surfaces but also in the optics of any surface waves on semiconductors and dielectrics.

We would like to acknowledge helpful discussions with Julius Goldhar and Saeed Pilevar.

[1] *Surface Polaritons,* edited by V. M. Agranovich and D. L. Mills (North-Holland, Amsterdam, 1982).
[2] O. Marti *et al.,* Opt. Commun. **96**, 225 (1993).
[3] P. M. Adam *et al.,* Phys. Rev. B **48**, 2680 (1993).
[4] P. Dawson *et al.,* Phys. Rev. Lett. **72**, 2927 (1994).
[5] S. I. Bozhevolnyi *et al.,* Phys. Rev. B **51**, 17 916 (1995).
[6] I. I. Smolyaninov *et al.,* Appl. Phys. Lett. **67**, 3859 (1995).
[7] I. I. Smolyaninov *et al.* (to be published).
[8] E. Kretschmann and H. Raether, Z. Naturforsch. A **23**, 2135 (1968).
[9] R. C. Reddick *et al.,* Phys. Rev. B **39**, 767 (1989).
[10] G. N. Zhizhin *et al.,* JETP Lett. **29**, 486 (1979).